THE JOURNAL OF PHYSICAL CHEMISTRY A

 VOLUME 111, NUMBER 43, NOVEMBER 1, 2007

ARTICLES

Ion-Pair Formation Dynamics of F_2 at 18.385 eV Studied by Velocity Map Imaging Method

Yusong Hao, Chang Zhou, and Yuxiang Mo*

Department of Physics and Key Laboratory for Atomic and Molecular Nanosciences, Tsinghua University, Beijing 100084, China

Received: June 20, 2007; In Final Form: August 12, 2007

We studied the ion-pair formation dynamics of F_2 at 18.385 eV (67.439 nm) using the velocity map imaging method. It was found that there are two dissociation channels corresponding to production of $F^+(^1D_2) + F^-(^1S_0)$ and $F^+(^3P_j) + F^-(^1S_0)$. The measured center-of-mass translational energy distribution shows that about 98% of the dissociation occurs via the $F^+(^1D_2)$ channel. The measured angular distributions of the photofragments indicate that dissociation for the $F^+(^3P_j)$ channel occurs via predissociation of Rydberg states converging to $F_2^+(\tilde{A}^2\Pi_u)$ and dissociation for the $F^+(^1D_2)$ channel involves mainly a direct perpendicular transition into the ion-pair state, or $X^1\Sigma_g^+ \rightarrow 2^1\Pi_u$, which is also supported by the transition dipole moment calculations .

Introduction

Ion-pair formation dynamics has recently attracted much attention.[1−11] However, there is not much information regarding the dynamics of ion-pair formation since there is still little detailed experimental research in comparison with photodissociation of neutral molecules. This is true even for diatomic molecules. Research on ion-pair formation dynamics should greatly increase our knowledge about the highly excited electronic states of molecules, in particular the so-called molecular superexcited states.[1−2]

Berkowitz et al. studied the ion-pair formation of F_2 by measuring the efficiency spectrum of producing F^+ (F^-) at different photon energies.[12] Their results showed that in the region 77.0−79.8 nm (16.10−15.54 eV) the efficiency spectrum consists of a very sharp resonance structure, which was explained by predissociation of Rydberg states into the ion-pair states correlating with $F^+(^3P)+F^-(^1S_0)$. The Rydberg states are converged to $F_2^+(\tilde{X}^2\Pi_g)$, which is the only energetically possible cation state in this region. In contrast, in the 64−68 nm (19.37−18.23 eV) region the efficiency spectrum is very broad and has only weak resonance structure. This was also explained by predissociation of Rydberg states, however, converging to $F_2^+(\tilde{A}^2\Pi_u)$. Berkowitz et al. guessed that the photofragments in this energy region may correlate with the channel of $F^+(^1D_2) + F^-(^1S_0)$. The predissociation mechanism is supported by the efficiency spectrum of producing F_2^+, which has a similar structure to that of the ion pair. However, direct measurement of the photofragment translational energy distribution would provide concrete evidence about the ion-pair formation channels, and measurement of the photofragment angular distribution would provide insight into the mechanism of ion-pair formation.

Recently, the velocity map imaging method[13] has been applied to study the ion-pair formation dynamics of CH_3F, CH_3Cl, CH_3Br, NO, O_2, F_2, and Cl_2.[3−8,10,11] In these studies, the translational energy distribution and angular distribution of the photofragments have been measured simultaneously. Therefore, deep insights into the dissociation dynamics have been obtained. In this paper, we present a study of F_2 ion-pair formation dynamics

* To whom correspondence should be addressed. E-mail: ymo@mail.tsinghua.edu.cn.

10.1021/jp074780a CCC: $37.00
Published on Web 10/11/2007

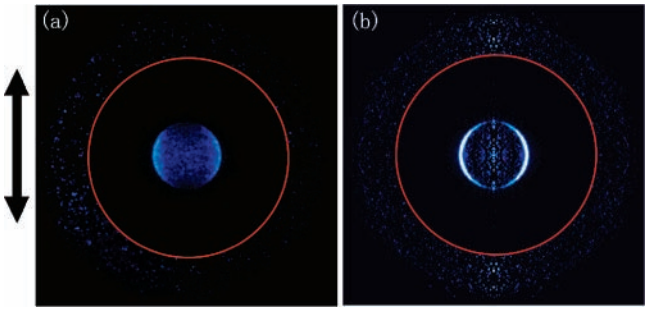

Figure 1. (a) Experimental raw image of F^- photofragment from F_2 ion-pair production at 18.385 eV under an electric field of 850 V/cm. The polarization of the XUV laser is parallel to the image plane and indicated in the figure. (b) 2-D slice of the reconstructed 3-D sphere from Abel−Hankel transform. The signal intensities outside the red circles have been increased by 30 times in order to show clearly the onsets of the channel $F^+(^3P_j) + F^-(^1S_0)$. The signals in the middle are from the channel $F^+(^1D_2) + F^-(^1S_0)$.

at 18.385 eV (67.439 nm) by recording the velocity map image of F^-, i.e.

$$F_2(X^1\Sigma_g^+) + 148\,282\ cm^{-1} \rightarrow F^+(^3P_j) + F^-(^1S_0) + 22\,240\ cm^{-1} \quad (1a)$$

$$\rightarrow F^+(^1D_2) + F^-(^1S_0) + 1367\ cm^{-1} \quad (1b)$$

Experimental Section

The experimental machine used in this study has been described in detail previously.[7,8] Only a brief summary is given here. The coherent XUV radiation ($3\omega_1$) was generated using the resonance-enhanced frequency tripling of a focused laser beam (ω_1) on a pulsed Kr jet. The fundamental laser beam (ω_1) was prepared by tripling of a dye laser, which was pumped by an Nd-YAG (20 Hz) laser. The $2\omega_1$ (98 855.1 cm^{-1}) was fixed at the transition of $4p^5(^2P_{1/2})5p[1/2]_0 \leftarrow (4p^6)^1S_0$. The apparatus consists of four vacuum chambers, namely, (a) a frequency mixing chamber, which houses the pulsed Kr jet (orifice diameter 1 mm), (b) a monochromator chamber, which is equipped with a gold-coated toroidal grating, (c) a molecular beam source chamber, which houses a pulsed valve (orifice diameter 0.7 mm) to produce a pulsed molecular beam (the beam enters into the ionization chamber through a skimmer (orifice diameter 1 mm)), and (d) an ionization chamber, which houses an electrostatic lens system for velocity map imaging[13] and a time-of-flight tube equipped with imaging quality dual MCP (ϕ50 mm and a channel pitch of 12 μm, North Night Vision, Nanjing Branch). The imaging plane is perpendicular to the molecular beam, and the distance from it to the interaction point between the XUV laser and molecular beam is 65 cm. The mass gate to select the F^- ion was a positive electric pulse of 100 ns width and 1500 V high provided by a high-voltage pulsed generator (PVM-4140, DEI). The ion images were captured by a deep cooled CCD camera with a resolution of 1024 × 1024 pixels[2] (Andor DU-434). The F_2 gas sample was premixed with He (He 96%, F_2 4%), and the stagnation pressure used was about 1000 Torr at room temperature. In the experiments, the pressures for the molecular beam source and ionization chamber were around 1×10^{-5} and 1×10^{-7} Torr, respectively.

Results and Discussion

Figure 1a shows the experimental raw image of F^- from F_2 ion-pair formation at a photolysis energy of 148 282 cm^{-1} (18.3846 eV or 67.439 nm) under an electric field of 850 V/cm, and Figure 1b shows the Abel−Hankel transform of Figure 1a. The polarization of the XUV radiation is also indicated in Figure 1. It is noted that in Figure 1a and 1b the signals outside the red circles have been increased by 30 times in order to clearly show the onsets of the photofragment signals. There are two components of signals with lower and higher velocities, which correspond to production of $F^+(^1D_2) + F^-(^1S_0)$ (eq 1a) and $F^+(^3P_j) + F^-(^1S_0)$ (eq 1b), respectively. The signals from the higher velocity components are very weak and have almost an isotropic angular distribution, while the signals from the lower velocity components are very strong and have an anisotropy angular distribution with the strongest signals at the direction perpendicular to the polarization direction of the XUV laser.

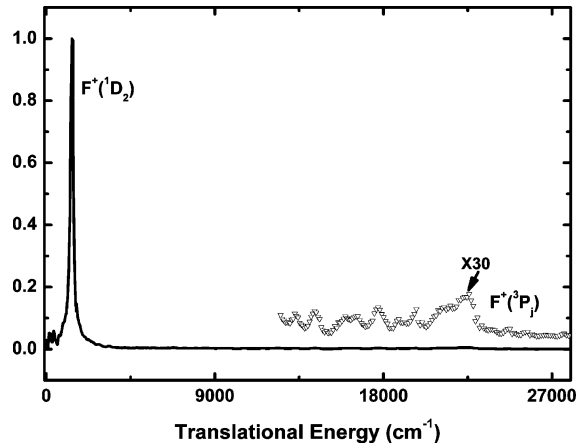

Figure 2. Center of mass translational energy distribution of photofragments for F_2 ion-pair production at 18.385 eV.

The threshold energy for ion-pair production (E_{tipp}) of F_2 has been determined as 12 6042 ± 8 cm^{-1} or 15.627 ± 0.001 eV by us previously.[7] For ion-pair formation occurring under an electric field the threshold will be lower due to the Stark effect. However, if the available energy for dissociation under zero field is much larger than the energy shift due to the Stark effect, which is true in our case, the ion-pair formation dynamics, such as the translational energy distribution and angular distribution of photofragments, should be affected very little.[8]

Figure 2 shows the center of mass (CM) translational energy distribution for F_2 ion-pair formation obtained from Figure 1b. In Figure 2 the strong peak corresponds to production of $F^+(^1D_2) + F^-(^1S_0)$ and the weak peak to production of $F^+(^3P_j) + F^-(^1S_0)$. Because of the very weak signals for the $F^+(^3P_j)$ channel we could not reliably resolved the three spin−orbit components of $F^+(^3P_{j=2,1,0})$. Table 1 lists the branching ratio of the $F^+(^1D_2)$ channel to $F^+(^3P_j)$ channel. It is seen that most of the photofragments are from the $F^+(^1D_2)$ channel.

The angular distributions for the channels corresponding to production of $F^+(^1D_2)$ and $F^+(^3P_j)$ can be extracted from Figure 1b, and they are shown in Figure 3, panels a and b, respectively. The anisotropy parameters β for the two channels are listed in Table 1. They are obtained using the following equation to fit the curves in panels a and b in Figure 3

$$f(\theta) \propto 1 + \beta P_2(\cos\theta) \quad (2)$$

where θ is the angle between the recoil velocity and the polarization direction of the XUV laser and $P_2(x)$ is the second-order Legendre polynomial. In the limiting case of parallel or perpendicular transitions for pure repulsive states, $\beta = 2$ or -1, respectively.[14] From Table 1 it is seen that the channel corresponding to production of $F^+(^1D_2)$ has a very large negative

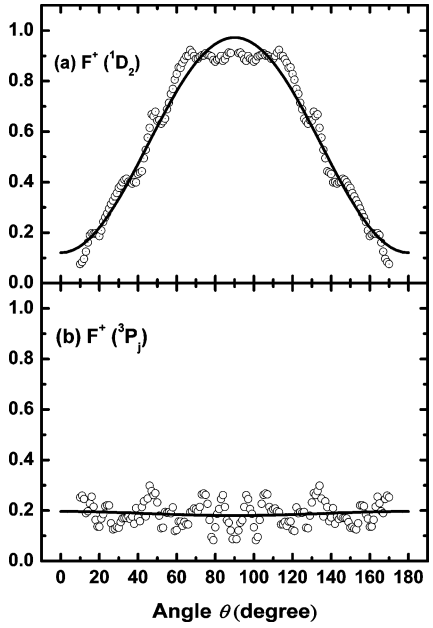

Figure 3. Angular distribution of F^- photofragments from F_2 ion-pair formation at 18.385 eV for the channels corresponding to production of (a) $F^+(^1D_2) + F^-(^1S_0)$ and (b) $F^+(^3P_j) + F^-(^1S_0)$. The small circles represent the experimental data, and the solid lines are the least-square fittings obtained using the anisotropy parameters β listed in Table 1.

TABLE 1: Anisotropy Parameters and Branching Ratio for Ion-Pair Formation,[a] $F_2(X^1\Sigma_g^+) \xrightarrow{18.385eV} F^+(^3P_j, ^1D_2) + F^-(^1S_0)$

channel	anisotropic parameter β	branching ratio
$F^-(^1S_0) + F^+(^1D_2)$	−0.82(5)	1.0
$F^-(^1S_0) + F^+(^3P_j)$	0.02(10)	0.02(2)

[a] The numbers in parentheses are uncertainties in the last two or one digits of the data, which are estimated by the signal-to-noise ratio of the experimental data.

β (−0.82 ± 0.05) and the channel corresponding to production of $F^+(^3P_j)$ has almost zero β (0.02 ± 0.10). The large negative β for the $F^+(^1D_2)$ channel means that dissociation occurs via a perpendicular transition and is very fast in comparison with the rotation period of F_2.[15] while the zero β for the $F^+(^3P_j)$ channel means that dissociation occurs via an intermediate state with lifetime much longer than the rotational period of F_2.[15]

The photon energy of 18.385 eV is too high to excite Rydberg states converging to $F_2^+(\tilde{X}^2\Pi_g)$since it would provide an available energy of 2.76 eV to excite F_2^+ $(\tilde{X}^2\Pi_g)$ in very high vibrational states, which is difficult due to the poor Franck−Condon factors associated with the corresponding transitions. However, it is possible to excite Rydberg states converging to $F_2^+(\tilde{A}^2\Pi_u)$ at 18.385 eV. From the isotropic angular distribution of the channel $F^+(^3P_j)$, it is known that the dissociation correlating with this channel should occur via a process with a lifetime much longer than the rotational period of F_2.[15] This slow process should be due to the predissociation of Rydberg states into the ion-pair state, and the Rydberg states should converge to $F_2^+(\tilde{A}^2\Pi_u)$. Nevertheless, further details about the properties of the related Rydberg states and the mechanism of predissociation from the singlet Rydberg state to the triplet ion-pair states are difficult to obtain based on the present experimental results only.

For the channel corresponding to production of $F^+(^1D_2)$ β approaches the limiting value of a fast perpendicular transition and the excited-state must be $^1\Pi_u$. However, this does not rule out dissociation occurring via a predissociation mechanism. Excitation to a Rydberg state of $^1\Pi_u$ symmetry converging to $F_2^+(\tilde{A}^2\Pi_u)$ is possible, for example, a Rydberg state of configuration $\pi_u^3\pi_g^4ns$, and the Rydberg state is then predissociated into the ion-pair state correlating with the $F^+(^1D_2)$ channel. Because most of the products are in the $F^+(^1D_2)$ channel, this mechanism would require a sharp resonance structure in the ion-pair efficiency spectrum, which is in contradiction to the experimental spectrum observed in the region 19.37−18.23 eV.[12]

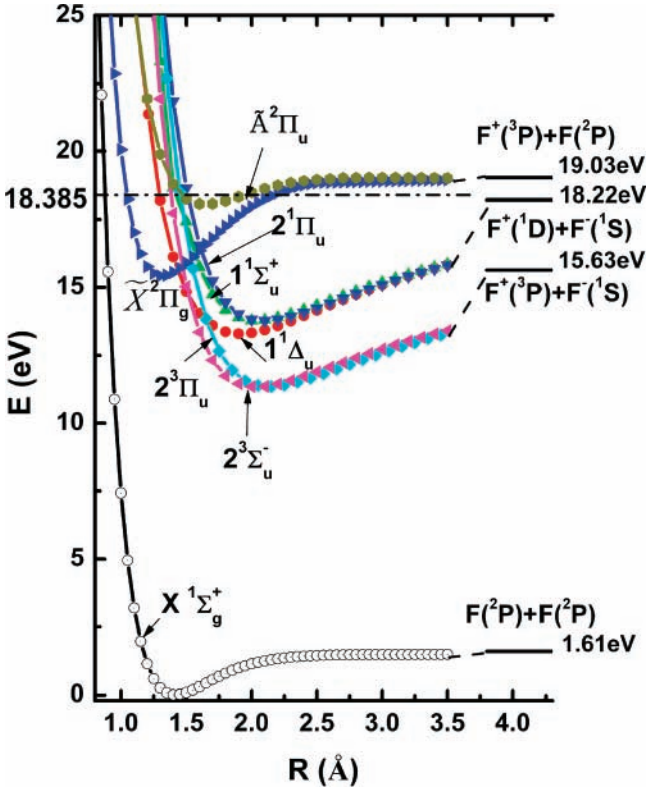

Figure 4. Calculated potential-energy curves of F_2 and F_2^+. Only ion-pair states that can be populated by one-photon excitation are shown. The indicated energy levels on the right-hand side are from the reported experimental data.[7,20]

To gain more insight into the ion-pair formation mechanism, the properties of the potential-energy curves (PECs) of ion-pair states should be very helpful. The PECs of F_2 correlating with $F^+(^3P_j) + F^-(^1S_0)$ have been reported.[16] Although there is no report about the PECs of F_2 correlating with $F^+(^1D_2) + F^-(^1S_0)$, detailed studies about the PECs of Cl_2 correlating with $Cl^+(^1D_2) + Cl^-(^1S_0)$ have been published.[17,18] Following their calculation methods, we calculated the PECs of ion-pair states of F_2 using the MOLPRO software package.[19] Only the PECs that can be populated by one-photon absorption are considered here. The calculation method is the so-called multireference internally contracted configuration interaction method (MRCI) with the basis set of aug-cc-pV5Z, and the reference functions for MRCI are from complete active space-SCF calculation (CASSCF). In the Franck−Condon region the interaction between the Rydberg states and the ion-pair states may occur, but this interaction was not given particular attention in our calculation. The PECs for $F_2^+(\tilde{X}^2\Pi_g)$ and $F_2^+(\tilde{A}^2\Pi_u)$ have been calculated also since Rydberg states converging to the two ionic states may be excited also. The results are shown in Figure 4. The energies shown on the right side in Figure 4 represent the energy levels of the corresponding PECs at infinite bond length, and they are from the experimental data.[7,20]

From Figure 4 it is seen that a photon energy of 18.385 eV can excite the vibrational ground state of $F_2(X^1\Sigma_g^+)$ into the

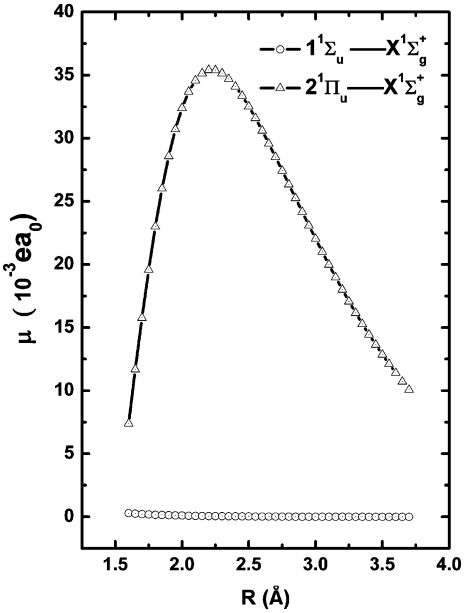

Figure 5. Calculated electronic transition dipole moments for one-photon transition from the ground electronic state to the ion-pair states correlating with $F^+(^1D_2) + F^-(^1S_0)$.

inner wall of the ion-pair states. Therefore, we believe that the channel corresponding to production of $F^+(^1D_2)$ is mostly from direct dissociation into the ion pair. In order to obtain further insight we calculated the electronic transition dipole moments to the ion-pair states correlating with the $F^+(^1D_2)$ channel. As shown in Figure 4, two possible ion-pair states correlating with the $F^+(^1D_2)$ channel, $1^1\Sigma_u^+$ and $2^1\Pi_u$, could be populated by one-photon excitation. The transition dipole moments from the ground state to these two states at different bond lengths are shown in Figure 5. The calculations have been done using the MOLPRO software package at the CASSCF/MRCI/aug-cc-pV5Z level. It is easily seen that the transition dipole moments to $2^1\Pi_u$ are much larger than those to $1^1\Sigma_u^+$, although the absolute values of the transition dipole moments to $2^1\Pi_u$ are small. Therefore, if direct excitation to the ion-pair states correlating to the $F^+(^1D)$ channel could occur, excitation should mainly occur via the $2^1\Pi_u$ state, which is a perpendicular transition. This is consistent with the experimental results. Therefore, calculation of the transition dipole moment demonstrates, in another respect, that ion-pair formation correlating with the $F^+(^1D)$ channel at 18.385 eV may occur via direct transition to the $2^1\Pi_u$ ion-pair state.

Although the efficiency spectrum of ion-pair production around 18.385 eV is broad as observed by Berkowitz et al.,[12] the dynamics of ion-pair formation may still vary with the excitation photon energies. To produce tunable XUV radiation by four-wave mixing in this energy region is very difficult at present;[21] we expect that future experiments could provide more insight into the ion-pair formation dynamics of F_2 using various excitation energies in this region.

Summary

We studied the ion-pair formation dynamics of F_2 at 18.385 eV (67.439 nm) using the velocity map imaging method. Two channels have been found, i.e.

$$F_2(X^1\Sigma_g^+) + 148282\ cm^{-1} \rightarrow F^+(^3P_j) + F^-(^1S_0) + 22240\ cm^{-1} \quad (1a)$$

$$\rightarrow F^+(^1D_2) + F^-(^1S_0) + 1367\ cm^{-1} \quad (1b)$$

The measured center-of-mass translational energy distribution shows that about 98% of the dissociation occurs via the $F^+(^1D_2)$ channel (eq 1b). The measured angular distributions of the photofragments indicate that dissociation for the $F^+(^3P_j)$ channel (eq 1a) occurs via predissociation of Rydberg states converging to $F_2^+(\tilde{A}^2\Pi_u)$ and dissociation for the $F^+(^1D_2)$ channel involves mainly a direct perpendicular transition into the ion-pair state or $X^1\Sigma_g^+ \rightarrow 2^1\Pi_u$, which is also supported by the calculation results about the transition dipole moments.

Acknowledgment. This work was funded by project 20673066 supported by the National Science Foundation of China, project 306020 supported by the Key grant Project of Chinese Ministry of Education, and Scientific Research Program of Tsinghua University.

References and Notes

(1) Hatano, Y. *J. Electron Spectrsoc. Relat. Phenom.* **2001**, *119*, 107.

(2) Suit, A. G.; Hepburn, J. W. *Annu. Rev. Phys. Chem.* **2006**, *57*, 431.

(3) Suto, K.; Sato, Y.; Reed, C. L.; Skorokhodov, V.; Matsumi, Y.; Kawasaki, M. *J. Phys. Chem. A* **1997**, *101*, 1222.

(4) (a) Ahmed, M.; Peterka, D. S.; Regan, P.; Liu, X. H.; Suits, A. G. *Chem. Phys. Lett.* **2001**, *339*, 203. (b) Liu, X. H.; Gross, R. L.; Suits, A. G. *Science* **2001**, *294*, 2527.

(5) Li, W.; Lucchese, R. R.; Doyuran, A.; Wu, Z.; Loos, H.; Hall, G. E.; Suits, A. G. *Phys. Rev. Lett.* **2004**, *92*, 083002.

(6) Xu, D.; Huang, J.; Price, R. J.; Jackson, W. M. *J. Phys. Chem. A* **2004**, *108*, 9916.

(7) (a) Yang, J.; Hao, Y.; Li, J.; Zhou, C.; Mo, Y. *J. Chem. Phys.* **2005**, *122*, 134308. (b) Yang, J.; Hao, Y.; Li, J.; Zhou, C.; Mo, Y. *J. Chem. Phys.*, in press.

(8) Hao, Y.; Zhou, C.; Mo, Y. *J. Phys. Chem. A* **2005**, *109*, 5832.

(9) Shaw, D. A.; Holland, D. M. P.; Walker, I. C. *J. Phys. B: At. Mol. Opt. Phys.* **2006**, *39*, 3549.

(10) Hikosaka, Y.; Kaneyasu, T.; Shigemasa, E. *J. Electron Spectrosc. Relat. Phenom.* **2007**, *154*, 43.

(11) Li, J.; Hao, Y.; Zhou, C.; Yang, J.; Mo, Y. *J. Chem. Phys.* ***2007***, *127*, 104307.

(12) Berkowitz, J.; Chupka, W. A.; Guyon, P. M.; Holloway, J. H.; Spohr, R. *J. Chem. Phys.* **1971**, *54*, 5165.

(13) Eppink, A. T. J. B.; Parker, D. H. *Rev. Sci. Instrum.* **1997**, *68*, 3477.

(14) Zare, R. N.; Herschbach, H. R. *Proc. IEEE* **1963**, *51*, 173.

(15) Yang, S.; Bersohn, R. *J. Chem. Phys.* **1974**, *61*, 4400.

(16) Delyagina, I. A.; Kokh, D. B.; Pravilov, A. M. *Mol. Spectrosc.* **2003**, *94*, 200.

(17) Peyerimhoff, S. D.; Buenker, R. J. *Chem. Phys.* **1981**, *57*, 279.

(18) Kokh, D. B.; Alekseyev, A. B.; Buenker, R. J. *J. Chem. Phys.* **2001**, *115*, 9298.

(19) Werner H.-J.; Knowles, P. J.; Lindh, R.; Manby, F. R.; Schutz, M.; et al., *MOLPRO*, version 2006.1, a package of *ab initio* programs; http://www.molpro.net.

(20) Sansonetti, J. E.; Martin, W. C. *Handbook of Basic Atomic Spectroscopic Data*; http://www.physics.nist.gov/PhysRefData/Handbook/index.html.

(21) Rupper, P.; Merkt, F. *Rev. Sci. Instrum.* **2004**, *75*, 613.